# Noise Temperature and Beam Pattern of a Quasioptical Heterodyne Receiver based on NbN Hot Electron Bolometer Mixer at 5.25 THz

W. Zhang[1,2,#], P. Khosropanah[1], J. R. Gao[1,3,*], T. Bansal[1,3], T. M. Klapwijk[3], W. Miao[2], and S. C. Shi[2]

[1]*SRON Netherlands Institute for Space Research, Groningen, the Netherlands*

[2]*Purple Mountain Observatory, National Astronomical Observatories of China, Chinese Academy of Sciences, China*

[3]*Kavli Institute of Nanoscience, Delft University of Technology, Delft, The Netherlands*

#Contact: wzhang@mail.pmo.ac.cn, phone +86-25-83332229

*Contact: J.R. Gao@tudelft.nl, phone +31-15-2781370

***Abstract*—We report the measured sensitivities of a superconducting NbN hot electron bolometer (HEB) heterodyne receiver at 5.25 THz. The terahertz (THz) radiation is quasi-optically coupled to the HEB mixer with a lens and a spiral antenna. Using a measurement setup with black body calibration sources and a beam splitter in vacuum, and an antireflection coated Si lens, we obtained a double sideband (DSB) receiver noise temperature ($T_{rec}^{DSB}$) of 1150 K, which is 4.5 times $h\nu/k$ (the quantum limit). In addition, the measured far field beam patterns of the integrated lens antenna from 2.5 THz to 5.3 THz show collimated beams that make it reliable to measure $T_{rec}^{DSB}$ using the vacuum setup. Our experimental results in combination with an antenna-to-bolometer coupling simulation suggest that the HEB mixer can work well at least up to 6 THz, suitable for next generation of high-resolution spectroscopic space telescopes and, in particular, for the detection of the neutral atomic oxygen (OI) line at 4.7 THz.**

## I. Introduction

Superconducting hot-electron bolometer (HEB) mixers are so far the most sensitive heterodyne detectors at THz frequencies above 1.5 THz. The HEB mixers based on NbN or NbTiN superconducting films have been successfully used to detect spectral lines up to 2 THz from ground based [1-3] and space [4] telescopes. The performances, such as the low double sideband (DSB) $T_{rec}^{DSB}$ of 1300 K at 4.3 THz [5], an intermediate frequency (IF) gain bandwidth of 3 GHz and noise bandwidth of ~5 GHz [6], low local oscillator (LO) power of 50-500 nW [7], and a long Allan variance stability time [1], have been reported by different research groups. They become the choice of the detector in the upper THz frequency range (3-6 THz) for high resolution spectroscopic observations for astronomy. One example is the fine-structure line of neutral atomic oxygen OI ($^3P_1$-$^3P_2$) at 4.7448 THz, which is a major coolant of dense interstellar medium and is a vital tool for probing the physical conditions of massive young stars [8]. The OI line has been recorded by a Schottky heterodyne receiver flying on the Kuiper Airbone Observatory [9]. However, the sensitivity of the receiver used is very poor and is 75000 K at 4.7 THz. The sensitivity of a receiver, i.e. $T_{rec}^{DSB}$, is a crucial parameter that defines the minimal detectable line amplitude and also the observation time.

The far field beam pattern of a quasi optical HEB mixer, governed by a lens/antenna combination and radiation frequency, is also an important performance parameter for a practical receiver. The beam pattern of a spiral antenna at 5 THz is not known, which motivates us to investigate that. Besides, we also notice that the beam patterns are crucial for measuring $T_{rec}^{DSB}$ when hot/cold loads with a limited surface area are used, which is the case in our vacuum setup.

The aim of this work is to demonstrate experimentally the ultimate sensitivity of an NbN HEB mixer at the high-end of THz frequency range. Here we use a similar HEB mixer and measurement setup as reported earlier at 4.3 THz [5]. However, we extend the LO frequency to 5.25 THz. We report $T_{rec}^{DSB}$ of 1150 K at 5.3 THz. In addition, the coupling efficiency between spiral antenna and bolometer is simulated. The far field beam patterns of the mixer were measured at several frequencies up to 5.3 THz.

## II. HEB Device and Measurement Setup

The HEB mixer used consists of 2 μm wide, 0.2 μm long, and 5.5 nm thick NbN bridge on a highly resistive Si substrate. The NbN thin film was produced by a group at Moscow State Pedagogical University (MSPU), Russia. The details of the NbN film can be found in [10]. The bridge is connected to the antenna by Nb (10 nm)/Au (50 nm) superconducting bilayer contact pads [11]. Prior to deposition of the contact pads, Ar ion etching is applied to clean the surface of NbN, eliminating contact resistance between NbN and contact pads. Such contact structures allow RF and DC power being dissipated only in the NbN bridge, thus there are no RF loss and no additional noise contribution due to the contact interface. The antenna is an on-chip self-complementary spiral antenna that is made of a 170 nm thick Au layer. It has a tight winding design with an inner diameter

of 6.6 μm close to the NbN bridge [Fig.1(a)]. The HEB has a low-temperature normal-state resistance ($R_N$) of 83 Ω, a critical temperature of 9.3 K, and a critical current of 210 μA at 4.2 K.

We apply the same vacuum measurement setup as described in [5] except for a different heat filter [12] and without bandpass filter. The HEB chip is glued to the backside of Si elliptical lenses [13] without and with an antireflection coating, mounted in a mixer unit that is placed in a 4.2-K liquid helium cryostat. As calibration sources, a blackbody at 295 K is used as the hot load and another one at 77 K as the cold load. The two loads can be selected by rotating a mirror. The radiation from the hot/cold load is combined with that from the LO by a 3-μm Mylar beam splitter. Before reaching the HEB, the radiation passes through the heat filter at 4.2 K that blocks infrared radiation. There is no window on the cryostat and all these components are in the same vacuum [14]. Therefore the radiation does not suffer from the absorption due to water in the air and due to the window.

The LO is an optically pumped FIR ring laser, operated at a frequency of 5.2456 THz using $CH_3OD$ gas, which is pumped by 9R08 $CO_2$ line. We choose this frequency because it provides enough amount of power in the frequency range of our interest. The LO power coupled to the mixer is regulated by rotating a wire grid in front of the gas laser

The IF signal, resulting from the mixing of the LO and the hot/cold load signal, first passes through a bias-T, a circulator, and then a cryogenic low noise amplifier (Berkshire 1.3-1.7 GHz) operated at 4.2 K, followed by room-temperature amplifiers. This signal is filtered at 1.5 GHz within a band of 80 MHz. Between each two components in the IF chain, an attenuator is added to avoid standing waves. The entire IF chain has a gain of about 80 dB and a noise temperature of 7 K.

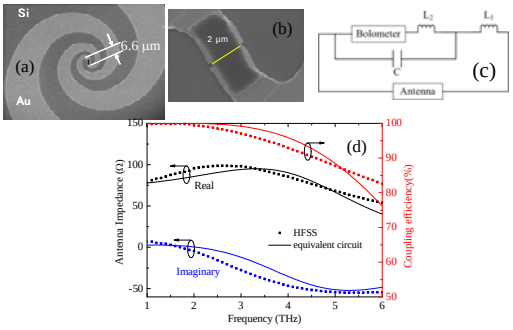


Fig. 1 (a) SEM picture of a tight winding spiral antenna with an inner diameter of 6.6 μm; (b) SEM picture of the NbN bridge with a length of 0.2 μm and a width of 2 μm; (c) Equivalent circuit of the whole antenna structure, which includes parasitic inductance and capacitance; (d) Simulated impedances of the spiral antenna versus frequency using HFSS and using the equivalent circuit (left axis) and calculated coupling efficiency between bolometer and antenna versus frequency (right axis).

## III. Simulation of the Antenna Impedance and the Coupling

To predict the impedance of the antenna and further calculate the coupling efficiency for the radiation power from the antenna to the HEB at the upper THz frequencies, we model the antenna using a three dimensional electromagnetic field simulator HFSS based on finite element method [15]. We assume that an RF signal is excited at the slit between two contact pads of the HEB, which is called lumped gap source. The Si substrate with a refractive index $n_{si}$=3.42 is set to be much thicker than the wavelength (λ) of the radiation and is treated as the half infinite space. All the surfaces are taken as radiation boundary. The scattering parameters are extracted from the electromagnetic field distribution. From the complex reflection coefficient ($S_{11}$) and its characteristic impedance ($Z_0$), the input impedance ($Z_{antenna}$) of the spiral antenna can be given as [16]:

$$Z_{antenna} = Z_0 \frac{1-S_{11}}{1+S_{11}} \qquad (1)$$

Fig. 1(d) shows the simulated $Z_{antenna}$ of the spiral antenna as a function of frequency between 1 and 6 THz. At lower frequencies the impedance is real and has a value close to 75 Ω, as expected for an equiangular spiral antenna [17]. But with increasing the frequency the reactive part appears and increases to -50 Ω at around 5 THz. The reactance can be explained by a parasitic effect that is due to the presence of a transition structure, namely the contact-pad structure between the HEB and the two arms of the spiral [see Fig.1(b)]. This leads to deformation of RF current and thus inductive and capacitive parasitic effects [18]. One can describe this by assuming an equivalent circuit that is shown in Fig.1(c). The transition structure acts as a series inductance $L_1$ to the antenna resistance $R_{antenna}$, and the slit between contact pads can be represented as a parallel capacitance $C$. Furthermore, the difference in the width between bolometer and contact pads causes current crowding which can be described as a series inductance $L_2$. Using this argument together with the following parameters: $R_{antenna}$=75 Ω, $L_1$=2.34 pH, $L_2$=0.7 pH, and $C$=0.45 fF, we can obtain a very similar impedance for the antenna as predicted by HFSS. The result is also plotted in Figure 1(d) for comparison.

Given that our HEB impedance is constant [19], equal to $R_N$, the coupling efficiency $\eta$ can be calculated based on the impedance match:

$$\eta = \frac{4Z_{HEB}\,re(Z_{antenna})}{\left|Z_{HEB}+Z_{antenna}\right|^2} \qquad (2)$$

The calculated $\eta$ is also given in Fig. 1(d). We find that $\eta$ is nearly 100 % at the frequencies below 3 THz, while above this value it decreases, but decreases gradually with increasing frequency. Even at the highest frequency of 6 THz, it is still more than 80 %, suggesting that our particular spiral antenna with the tight winding design can work well up to at least 6 THz and even beyond this frequency. For comparison, Fig. 1(d) shows also the calculated coupling efficiency based on the simple equivalent circuit. The result suggests that the simple model is able to qualitatively explain the frequency dependence of $\eta$.

## IV. Characterizing an Anti-Reflection Coated Lens

It is known that when a Si lens is used to couple THz radiation from the free-space to an antenna, a considerable amount of optical loss is due to reflection because of the high reflective index of Si, $n_{si}$. This loss can be minimized by coating an anti-reflection layer with a thickness of quarter wavelength ($\lambda/4n_{AR}$) and with a refractive index $n_{AR} = \sqrt{n_{si}} = 1.85$. Parylene C is a known coating material since it has a refractive index ($n_{PC}$) of 1.65, which is close to the optimum value [20].

To measure the ultimate $T_{rec}^{DSB}$ at 5.25 THz, we apply an existing Si lens coated with a Parylene C. The coating layer has a thickness of 10.9 μm and was originally designed for 4.3 THz [5]. To find its transmission at 5.25 THz, we prepared a double-side polished Si wafer coated with a Parylene C layer of the same thickness (10.9 μm) on both sides and measured the power transmission as a function of frequency by a Fourier transform spectrometer. The measured result is shown in Fig. 2. A good theoretical fit to the measured data is found when the coating layer is assumed to be 10.93 μm thick and $n_{PC}=1.634$. Based on the data and analysis, the transmission for the coated lens as a function of frequency is calculated and also depicted in Fig. 2. At 5.25 THz the transmission reaches 92 %, which is 22 % higher compared to that of an uncoated lens. We also find that at the designed frequency (4.3 THz), the transmission reaches its maximum of 97 %.

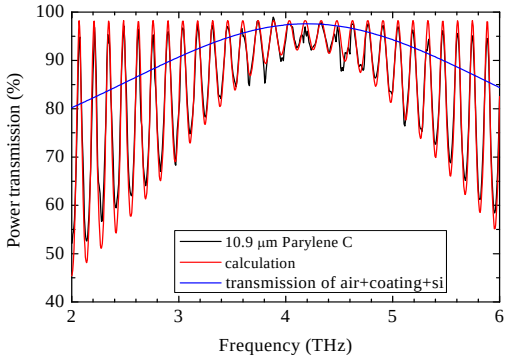


Fig. 2 Measured and theoretical power transmission of a double-side polished Si wafer coated with a Parylene C layer on both sides. The Si wafer and Parylene C coating layer are 2 mm and 10.9 μm thick, respectively.

## V. Experimental Results

### A. R-T Curve and Pumped I-V Curves

The resistance of a similar HEB from the same fabrication run has been measured as a function of temperature. The result is shown in the inset of Fig. 3. It is featured by three superconducting transitions. The lowest transition $T_{c1}$ of 6 K is associated to the Au/Nb/NbN contact structures; the middle transition $T_{c2}$ of 8 K is associated to the NbN under Au (thick) antenna layer; and the highest transition $T_{c3}$ of 9.3 K is due to the NbN bridge. The resistance above $T_{c3}$ is about 83 Ω, making a good impedance match possible with the spiral antenna. It is important to mention that in our case when the HEB is operated in the optimal biasing point, the contacts are in the superconducting state. More discussions of the superconducting transitions in such structures can be found elsewhere [11].

A typical set of I-V curves of the HEB with different LO power levels at 5.25 THz, recorded at 4 K, are shown in Fig. 3. With increasing LO power level, the superconductivity of the NbN bridge becomes gradually suppressed, showing a transition from the superconducting state to normal. The measured curves can be explained by a nonuniform distribution model for a HEB [21]. The optimum operating region, where the lowest $T_{rec}^{DSB}$ can be obtained, is indicated in the I-V plot. This region is centered around a bias voltage of 0.6 mV and a current of 34 μA. The optimum LO power in the HEB is about 150 nW, obtained by the isothermal technique [22]. The LO power required for HEB is known to be proportional to the volume and the $T_{c3}$ of the HEB.

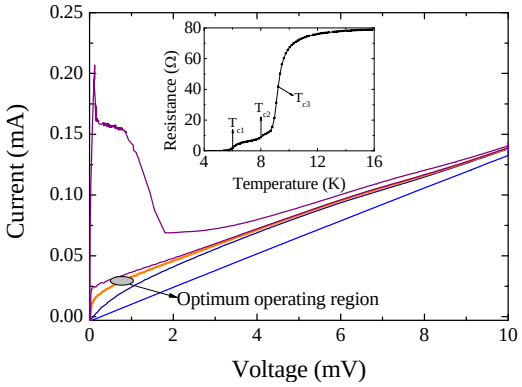


Fig. 3 A set of current-voltage curves of the NbN HEB mixer at 4.2 K and at different LO power, where the optimum operating region is indicated. The inset shows the DC resistance versus temperature of a very similar HEB, which was measured in the low current limit.

### B. Receiver Noise Temperature at 5.25 THz

We start with a measurement in which the HEB is mounted on the uncoated Si lens and $T_{rec}^{DSB}$ is characterized in a conventional way. We measured the output power of the receiver, $P_{out,hot}$ and $P_{out,cold}$, responding to the hot and cold load as a function of bias voltage under a constant, but optimum LO power. The results are plotted in Fig. 4. $T_{rec}^{DSB}$ is obtained by the Y-factor method and using the equivalent temperatures for the blackbody at 295 K and 77 K according to Callen-Welton definition [23]. $T_{rec}^{DSB}$ as a function of bias voltage is also plotted in Fig. 4. The lowest $T_{rec}^{DSB}$ (black dot line) is roughly 2000±500 K. The uncertainties are mainly caused by the LO power fluctuation and drift.

It has been well established that a HEB with a wideband antenna and low LO power requirement can suffer from the direct detection effect due to broadband blackbody radiation [24]. An additional demonstration of the direct detection effect in this particular experiment will be given in the subsection C. As a result, a measured $T_{rec}^{DSB}$ is usually higher than it should be [25]. This effect can be corrected out by adjusting LO power such that the DC current of the HEB is the same responding to the hot and cold loads. For comparison, the receiver output power data after adjusting

LO power are also shown in Fig. 4. For clarity a 2 dB positive offset in the vertical direction is introduced in the plot. The measured lowest $T_{rec}^{DSB}$ becomes 1500±300 K, which is on average 25% lower than what measured previously.

By applying a different characterization method [5] we can measure directly $T_{rec}^{DSB}$, without suffering from the direct detection and the instability of the gas laser as well. At the bias voltage of 0.6 mV we measure the receiver output power as a function of bias current, which is the result of varying LO power. Two such data sets are recorded, $P_{out,hot}(I)$ responding to the hot load and $P_{out,cold}(I)$ to the cold load. The Y factor can be obtained by $Y(I)= P_{out,hot}(I)/P_{out,cold}(I)$ at the same current using the fitted polynomial curves. The calculated $T_{rec}^{DSB}$ as a function of bias current is plotted in Fig. 5 and shows a broad minimum at the bias current of around 34 μA and the lowest value of 1550±50 K. This is in good agreement with the value measured in the conventional way, but after correcting the direct detection effect. The advantage is the high accuracy. Furthermore, the mixer conversion loss is found to be 8.9 dB.

Now we measure $T_{rec}^{DSB}$ of the same HEB, but mounted on the coated Si lens. Again, we measure at the optimum bias voltage of 0.6 mV. The data are added in Fig. 5. For clarity, the receiver output power data as a function of current, responding to hot/cold loads, have an offset positively by 2 dB. The lowest $T_{rec}^{DSB}$ obtained is 1150±40 K, which is about 23 % lower than the value (1550 K) measured previously using the uncoated lens. This difference is consistent with what is expected from using anti-reflection coating.

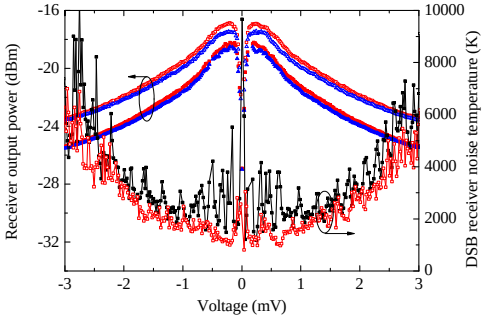


Fig. 4 Measured receiver output power (left axis) responding to the hot and cold load at optimum LO power as a function of bias voltage. One set of data are measured with fixed LO power level, and another set (2 dB positive offset for clarity) by adjusting LO power such that the current is the same for hot and cold loads. The resulted DSB receiver noise temperatures are also plotted vs. bias voltage (right axis).

### C. Direct Detection

Fig. 6 shows measured receiver output power, together with the DC current of the HEB, as a function of time over a period of 150 seconds, during which the hot and cold loads are manually switched after roughly each 5 seconds. The HEB in this case is mounted on the coated lens. The bias voltage is fixed at 0.8 mV and the LO power set at the optimal value. The periodic jumps of ≤ 0.3 dB in the output power between the hot and cold load should reflect directly how large the Y-factor is. However, the actual value is affected by the direct detection effect [25]. This effect is demonstrated by the observed jumps in the current, which is about 1.2 μA in amplitude. In principle, the direct detection effect can be minimized or eliminated by reducing the blackbody radiation power, for example, by adding a narrow bandpass filter in front of the mixer [24].

The absolute value of the bias current corresponding to either the hot or cold load varies less than 2 % during the measurement period in Fig. 6, which indicates reasonable power stability of the 5.25 THz lasing line.

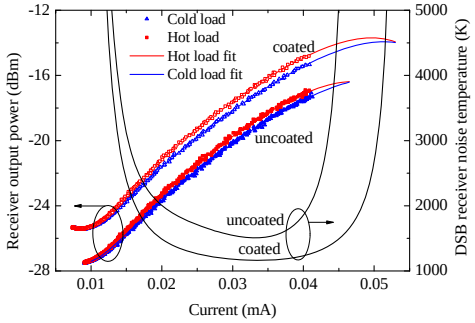


Fig. 5 Measured receiver output powers at the optimum bias voltage of 0.6 mV (dots) and the polynomial fit (lines) responding to the hot and cold load as a function of bias current of the HEB, which is varied by changing the LO power (left axis). One set of data are measured using uncoated lens and another set of data (2 dB positive offset for clarity) are measured using a coated lens. The resulted DSB receiver noise temperature curves are also shown as a function of bias current of the HEB (right axis).

### D. Beam Patterns of the Lens/Antenna

The far-field beam patterns of the same HEB mixer on the uncoated Si lens are measured at several frequencies from 2.5 to 5.3 THz using a computer controlled setup as described previously [26]. We apply the same gas laser as a signal source to measure the beams of the mixer. The HEB cryostat is placed on a rotation/tilt table in the far-field of the gas laser, which has a linearly polarized electrical field in the vertical direction. The center of the spiral antenna is located in the axis of the rotation.

The HEB is heated to a temperature which is slightly below the superconducting transition temperature of the NbN bridge $T_{c3}$. It is voltage biased and the current changes due to the modulated incident power are measured as a function of the angle of rotation/tilt by a lock-in amplifier. The tilt movement is referred to as vertical scan and the rotation as horizontal scan. The dynamic range of the setup is about 20 dB. The antenna is positioned in such a way that the direction along the NbN bridge width is about 30 degrees counter clockwise from the vertical direction of the setup.

Fig. 7 shows the beam patterns, measured in both horizontal and vertical directions of the integrated lens/antenna at 2.5 THz, 4.3 THz and 5.3 THz. The main lobes are similar in horizontal and vertical scans, which indicate that our beam patterns are close to rotational symmetry. The full width half maximum (FWHM) at 5.3 THz is 0.6 degree, which is similar to 0.55 degree at 4.3 THz, but smaller than 0.9 degree at 2.5 THz. At such high

frequencies the beam pattern of integrated lens antenna is diffraction limited, which scales with the wavelength and the effective aperture. The main beam becomes narrower from 2.5 to 4.3 THz due to wavelength, while it is almost the same between 4.3 THz and 5.3 THz, indicating the effective aperture at 5.3 THz is smaller. The difference in the side lobes is likely due to combination of antenna misalignment, IF feed structure and the measurement setup. Especially at 5.3 THz the beam profile in vertical scan has a large shoulder [see Fig. 7(c)], the reason for which is unclear yet. The first side lobes at 2.5 THz, 4.3 THz and 5.3 THz occur at -13, -11 and -7 dB, respectively, which increases with increasing the frequency [27]. The physical reasons of this are the internal reflection and surface roughness [28], [29]. Although the beam patterns are not ideally Gaussian, the measured beam patterns of the lens/antenna combination confirm the collimated beam, which is crucial to correctly measure $T_{rec}^{DSB}$ using the vacuum setup.

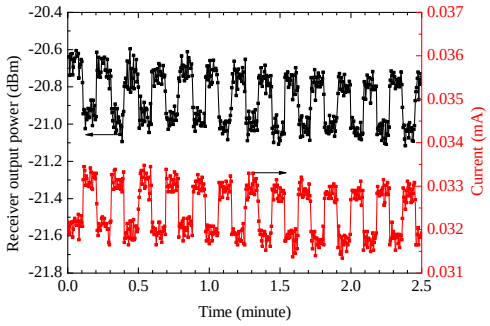


Fig. 6 Measured receiver output power, together with the bias current of the HEB, is measured as a function of time over a period of 150 seconds, during which the hot and cold load are manually switched after roughly each 5 seconds.

## VI. Conclusions

We have demonstrated a highly sensitive NbN HEB mixer at 5.25 THz using a spiral antenna coupled NbN HEB. We measured the lowest $T_{rec}^{DSB}$ of 1150 K at 5.25 THz. It is worthwhile to note that the sensitivity at 5.3 THz is about 65 times better than the Schottky diode mixer at 4.7 THz [9]. We also present the far-field beam pattern of the mixer at 5.25 THz, which shows a collimated beam with the side lobe occurring roughly at -7 dB level. With further improvement of the beam pattern, such a mixer together with recently developed THz quantum cascade lasers as LO should allow constructing new receivers [30] for detecting OI line at 4.7 THz for future airborne and space-borne telescopes.

## Acknowledgment

We acknowledge E.L. Kollberg and K.S. Yngvesson for stimulating discussions on the equivalent circuit of the antenna, L. de Jong, W. M. Laauwen, and J. N. Hovenier for their technical support, and W. Horinga for the FTS transmission measurement. The work was supported by the NSFC under Grant Nos. 10803021 and 10621303, and by China Exchange Programme executed by KNAW and CAS, and by the AMSTAR+ project of RadioNet under FP7 and N.W.O.

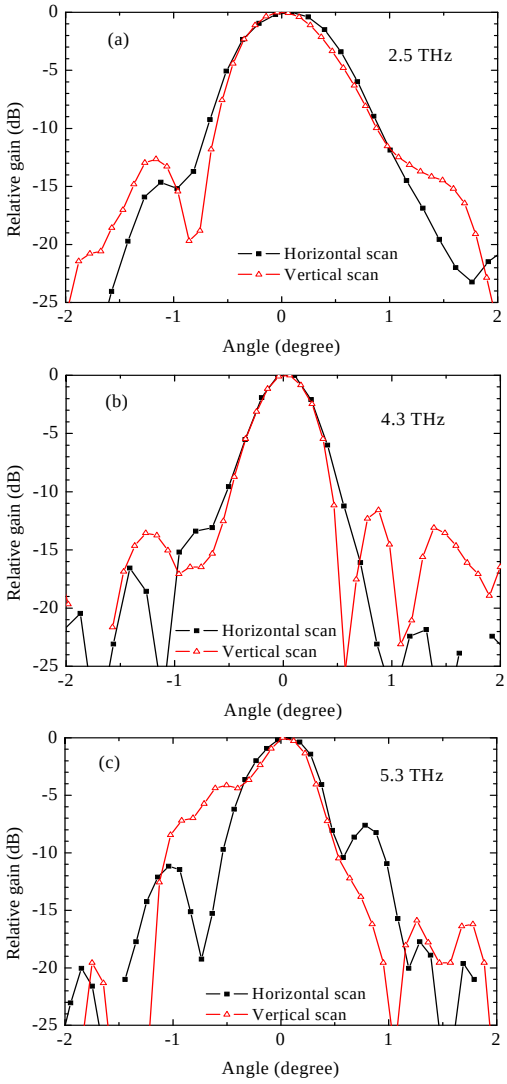


Fig. 7 Measured far field beam patterns of the HEB mixer on the uncoated Si lens, which are the same as used for the sensitivity measurements, at 2.5 THz (a), 4.3 THz (b), and 5.3 THz (c). The scans are made for both horizontal and vertical directions. The horizontal scan is indicated by black solid square+line; while the vertical scan by red hollow triangle+line.

## References

[1] D. Meledin, A. Pavolotsky, V. Desmaris, I. Lapkin, C. Risacher, V. Perez, D. Henke, O. Nystrom, E. Sundin, D. Dochev, M. Pantaleev, M. Fredrixon, M. Strandberg, B. Voronov, G. Goltsman, and V. Belitsky, IEEE Trans. Microwave Theory Tech. **57**, 89 (2009).

[2] J. Kawamura, R. Blundell, C.-Y. Tong, D. Papa, T. Hunter, G. Goltsman, S. Cherednichenko, B. Voronov, and E. Gershenzon, Proceedings of 9th International Symposium on Space Terahertz Technology, Pasadena, California, USA, 17-19 March 1998 (unpublished), pp. 35-43.

[3] M. C. Wiedner, G. Wieching, F. Bielau, K. Rettenbacher, N. H. Volgenau, M. Emprechtinger, U. U. Graf, C. E. Honingh, K. Jacobs, B. Vowinkel, K. M. Menten, L.-A. Nyman, R. Gusten, S. Philipp, D. Rabanus, J. Stutzki, and F. Wyrowski, A&A., **454**, L33 (2006).

[4] S. Cherednichenko, V. Drakinskiy, T. Berg, P. Khosropanah, and E. Kollberg, Review of Scientific Instruments, **79**, 0334501 (2008).

[5] P. Khosropanah, J. R. Gao, W. M. Laauwen, M. Hajenius, and T. M. Klapwijk, Appl. Phys. Lett. **91**, 221111 (2007).

[6] J. W. Kooi, J. J. A. Baselmans, J. R. Gao, T. M. Klapwijk, M. Hajenius, P. Dieleman, A. Baryshevm, and G. de Lange, J. Appl. Phys. **101**, 044511 (2007).

[7] S. Cherednichenko, P. Khosropanah, E. Kollberg, M. Kroug, H. Merkel, Physica C, **372-376**, 407 (2002).

[8] R. Gusten, P. Hartogh, H.-W. Hubers, U. Graf, K. Jacobs, H.P. Poser, F. Schafer, R. Schieder, R. Stark, J. Stutzki, P. Van der Wal, and A. Wunsch, Proc. SPIE, **4014**, 23 (2000).

[9] R. T. Boreiko and A.L. Betz, ApJ, **464,** L83 (1996).

[10] J. R. Gao, M. Hajenius, F. D. Tichelaar, T. M. Klapwijk, B. Voronov, E. Grishin, G. Gol'tsman, C. A. Zorman and M. Mehregany, Appl. Phys. Lett. **91**, 062504 (2007),

[11] T. Aggarwal, P. Khosropanah, W. Zhang, F. D. Tichelaar, J. R. Gao, and T. M. Klapwijk, Proceedings of 19th International Symposium on Space Terahertz Technology, Groningen, The Netherlands, 28-30 April 2008 (unpublished), pp.398-402.

[12] The heat filter has an upper cutoff frequency of 6 THz and 0.8 dB loss at 5.25 THz and is produced by QMC Ltd.

[13] HEB chip is placed on the backside of an elliptical Si lens, which is governed by the equation of $(x/a)^2+(y/b)^2=1$ with a major radii b=5.228 mm and a minor radii a=5 mm. The extension from geometric center of the elliptical lens is 1.229 mm and the Si substrate of the HEB chip is 340 μm thick.

[14] Vacuum unit consists of a beam splitter (which is changeable), a hot and cold load, and a rotating mirror. The beam splitter (3-μm Mylar) with a diameter of 22 mm is 35 mm away from the cryostat (the position of the window if it is there). The hot and cold load with diameters of 30 mm are 140 mm and 230 mm, respectively, away from the cryostat.

[15] 3D Full-wave Electromagnetic Field Simulation, see http://ansoft.com/products/hf/HFSS/.

[16] W. Zhang, C-.Y. Edward Tong, and S. C. Shi, IEEE Microwave & Wireless Components Letts. **13**, 376 (2003).

[17] J. D. Dyson, IRE Trans. Antennas and Propagation, **7**, 181 (1959).

[18] P. Focardi, A. Neto, W. McGrath, IEEE Trans. Microwave Theory Tech. **50**, 2374 (2002).

[19] E. L. Kollber, K. S. Yngvesson, Y. Ren, W. Zhang, P. Khosropanah, and J. R. Gao, (unpublished).

[20] H.-W. Hüber, J. Schubert, A. Krabbe, M. Birk, G. Wagner, A. Semenov, G. Goltsman, B. Voronov and E. Gershenzon, Infrared Physics & technology, **42**, 41 (2001).

[21] R. Barends, M. Hajenius, J. R. Gao, and T.M. Klapwijk, Appl. Phys. Lett. **87**, 263506 (2005).

[22] H. Ekstrom, B. Karasik, E. Kollberg, and S. Yngvesson, IEEE Trans. Microwave Theory Tech. **43**, 938 (1995).

[23] A. R. Kerr, IEEE Trans. Microwave Theory Tech. **47**, 325 (1999).

[24] M. Hajenius, J. J. A. Baselmans, A. Baryshev, J. R. Gao, T. M. Klapwijk, J. W. Kooi, W. Jellema, and Z. Q. Yang, J. Appl. Phys. **100**, 074507 (2006).

[25] J. J. A. Baselmans, A. Baryshev, S.F. Reker, M. Hajenius, J.R. Gao, T.M. Klapwijk, B. Voronov, and G. Goltsman, J. Appl. Phys. **100**, 084510 (2006).

[26] P. Yagoubov, W.J. Vreeling, and P.de Korte, Proceedings of 12th International Symposium on Space Terahertz Technology, San Diego, California, 14-16 February 2001(unpublished), pp.193-199.

[27] H.-W. Hüber, A. D. Semenov, H. Richter, J. Schubert, S. Hadjiloucas, J. W. Bowen, G. N. Goltsman, B. M. Voronov, and E.M. Gershenzon, Proceedings of 12th International Symposium on Space Terahertz Technology, San Diego, California, 14-16 Feb 2001, pp.286-296.

[28] M. J. M. van der Vorst, P. J. I. de Maagt, A. Netto, A. L. Reynolds, R. M. Heeres, W. Luinge, and M. H. A. J. Herben, IEEE Trans. Microwave Theory Tech. **49**, 1118 (2001).

[29] A. D. Semenov, H. Richterm H.-W. Hübers, B. Gunther, A. Smirnov, K. S. Il'in, M. Siegel and J. P. Karamarkovic, IEEE Trans. Microwave Theory Tech. **55**, 239 (2007).

[30] J. R. Gao, J. N. Hovenier, Z. Q. Yang, J. J. A. Baselmans, A. Baryshev, M. Hajenius, T. M. Klapwijk, A. J. L. Adam, T. O. Klaassen, B. S. Williams, S. Kumar, Q. Hu, and J. L. Reno, Appl. Phys. Lett. **86**, 244104, 2005.